Journal of Molecular Graphics and Modelling 27 (2009) 620–627

Contents lists available at ScienceDirect

Journal of Molecular Graphics and Modelling

journal homepage: www.elsevier.com/locate/JMGM

A DFT study of the ^{67}Zn, ^{14}N and ^{2}H electric field gradient tensors in Zinc(II)–4-MeIm complexes and extrapolation to superoxide dismutase

S. Javadian [a,*], R. Araghi [b]

[a] Department of Chemistry, Tarbiat Modarres University, P.O. Box 14155-4838, Tehran 14115-175, Iran
[b] Department of Chemistry, Payam Nour University, Tehran, Iran

ARTICLE INFO

Article history:
Received 13 May 2008
Received in revised form 8 October 2008
Accepted 9 October 2008
Available online 17 October 2008

Keywords:
DFT
4-Methyl imidazole
NQR parameters
Superoxide dismutase
Metal–ligand interactions

ABSTRACT

A computational investigation was carried out to characterize the ^{14}N and ^{2}H electric field gradient, EFG, in four protonated forms of 4-methyl imidazole (4-MeIm) and Histidine. In an attempt to establish metal binding effect in biological systems, we have considered the various forms of zinc (II) complexes of 4-MeIm. The computations were performed at the B3LYP and PW91P86 levels with 6-311++G(d,P) standard basis set. Calculated EFG tensors were used to determine ^{14}N and ^{2}H nuclear quadrupole coupling constant, χ and asymmetry parameter, η. The results show that Zn^{2+} has a strong effect on the NQR parameters (χ, η) of proximal nitrogen in contrast with the remote nitrogen. In addition, EFG tensors at the Zn nuclear site were calculated for Zn–4-MeIm complexes and estimated the χ and η values of ^{67}Zn. The influence of the bulk solvent was investigated at the B3LYP/6-311++G(d,p) level using the polarizable continuum model. Finally, we predicted (χ = 1.95 MHz, η = 0.84) for proximal nitrogen, (χ = 2.38 MHz, η = 0.07) for remote nitrogen and (χ = 1.28 MHz, η = 0.22) for Zn in superoxide dismutase.

1. Introduction

Imidazole is a fundamental component of many proteins, in particular as a constituent of the amino acid histidine [1]. It can act as a general acid or base to protonate or deprotonate the substrate. In addition, evidence suggests that it is involved in hydrogen bonding interactions that stabilize transition states and organize the active center of enzymes [2–4]. Moreover, imidazole nitrogens in the side chains of proteins can act as binding sites for metal ions [5–8]. Indeed, imidazole nitrogens play an important role in the functioning of many metalloenzyme systems. Their involvement is particularly noticeable, for example, in the binding of zinc to carboxy peptidase [9], carbonic anhydrase [10] and superoxide dismutase [11]. Therefore, knowledge of the coordination and protonation state of histidine ligands is needed if we are to understand the reaction mechanisms of metalloenzymes.

In recent years, experimental approaches such as nuclear magnetic resonance (NMR), nuclear quadrupole resonance (NQR), Raman and IR spectroscopy have been used to investigate various properties of histidine, including the protonation states, metal binding characteristics, and hydrogen bonding interactions [12–16]. In addition, quantum mechanical calculations have been used to study the role of imidazole in proton transfer in enzymatic reactions and as a ligand in metalloenzymes [17–21].

The present study focuses on the calculation and interpretation of NQR parameters associated with the ^{14}N, ^{67}Zn and ^{2}H nuclei in various protonation and Zn(II) complex forms of 4-methylimidazole (4-MeIm). NQR parameters provide a measure of the coupling between the nuclear quadrupole moments of quadrupole nuclei (spin $I > 1/2$) and the electric field gradient (EFG) at a given nucleus site due to the nonspherical charge distribution in the system. Such interactions can be measured either in the gas phase (using microwave spectroscopy) or in the solid state (mostly by NQR spectroscopy) [22,23].

The NQR parameters of ^{14}N atoms are good indicators of the protonation states of 4-MeIm and can provide useful information about hydrogen bonding interaction. These parameters can also be used to make quite detailed inferences about electron transfer in the binding of 4-MeIm to a metal center. However, several theoretical studies of NQR parameters have been performed on imidazole, its derivatives and complexes with metal ions. Fritscher studied the influence of hydrogen bond geometry on ^{14}N quadrupole interactions in imidazole–water and methyl imidazole–benzosemiquinone systems [24]. In another work in this area, the ^{14}N and ^{2}H quadrupole interaction parameters in a variety of substituted imidazoles were used to determine the crystal

* Corresponding author. Fax: +98 21 82883455.
E-mail addresses: javadian_s@modares.ac.ir, javadians@yahoo.com (S. Javadian).

1093-3263/$ – see front matter © 2008 Elsevier Inc. All rights reserved.
doi:10.1016/j.jmgm.2008.10.001

structure and to confirm the existence of intermolecular hydrogen bonding [25–27]. In addition, Morokuma et al. investigated the ^{14}N NQR parameters of a series of imidazole derivatives in different environments in both the gas phase and the solid state [28]. Mohebbi et al. studied the influence of the metal–ligand interactions on the NQR parameters of ^{14}N in *P. falciparum* histidine-rich protein–ferriprotoporphyrin IX complex (PfHRP2–Fe^{3+}-PPIX). They found that the binding of Fe^{3+}-PPIX to PfHRP2 in the PfHRP2–Fe^{3+}-PPIX complex has a significant effect in χ and in particular η of nitrogen [29]. To the best of our knowledge, no theoretical study has been reported for the NQR parameters of ^{14}N, ^{67}Zn and ^{2}H in various forms of Zn(II)–4-MeIm complexes. In the present study, the ^{14}N and ^{2}H NQR parameters were evaluated for various protonation forms of 4-MeIm and histidine using density functional theory (DFT). The present findings provide the theoretical basis for utilizing NQR parameters as indicators of the protonation of histidine. In addition, we extended the study to include various coordination forms of 4-MeIm to Zn(II) and conclude the paper with a final section devoted to the simulation of metal ligand interactions in real biomolecular systems like superoxide dismutase.

2. Theory

The quadrupolar Hamiltonian, H_Q, describes the interaction of the quadrupole moment, eQ, of a nucleus with spin greater than 1/2 with the EFG at the nuclear site. The Hamiltonian in the principal axes system (PAS) may be written as

$$\hat{H}_Q = \frac{e^2 Q q_{zz}}{4I(2I-1)}[(3\hat{I}_z^2 - \hat{I}^2) + \eta(\hat{I}_x^2 - \hat{I}_y^2)] \quad (1)$$

Then, using the raising and lowering operators, $\hat{I}_\pm$, the following equation can be derived in a straightforward manner:

$$\hat{H}_Q = \frac{e^2 Q q_{zz}}{4I(2I-1)}[(3\hat{I}_z^2 - \hat{I}^2) + \frac{\eta}{2}(\hat{I}_+^2 + \hat{I}_-^2)] \quad (2)$$

where q_{ij} are the components of the EFG tensor. As the EFG tensor is a traceless, symmetric second rank tensor, its principal axes are chosen so that its components satisfy $|q_{zz}| \geq |q_{yy}| \geq |q_{xx}|$, ($q_{ij} = \partial^2 V / \partial i \partial j$, where $i,j = x$, y and z, and V is the external electrostatic potential). η is an asymmetry parameter, $\eta = |(q_{xx} - q_{yy})/q_{zz}|$ and $\hat{I}$ is the spin quantum number of nuclei, where $\hat{I}_z$, $\hat{I}_x$ and $\hat{I}_y$ are the Z, X and Y components of the angular momentum [30].

The value of the nuclear quadrupole coupling constant ($\chi = e^2 Qq/h$) is calculated from the principal components of the EFG tensor, where Q is the nuclear electric quadrupole moment and $q = q_{zz}$. The electric quadrupole moments of ^{2}H, ^{67}Zn and ^{14}N are taken as $Q = 2.86$, 1.50, and 20.44 mb, respectively [31].

3. Computational methods

The DFT calculations were carried out using the Gaussian 98 suite of programs [32] and the geometry optimization was performed at the B3LYP/6-31G(d,p) level. To evaluate and ensure the optimized structures of the molecules, frequency calculations were carried out using analytical second derivatives. In all cases, only real frequencies were obtained for the optimized structures.

To calculate the ^{14}N, ^{67}Zn and ^{2}H EFG tensors in the principal axis system (PAS), two levels of DFT methods including B3LYP [33,34] and PW91P86 [35] with the basis set of 6-311++G(d,p) were employed. Recent studies suggest that the B3LYP and PW91P86 levels of theory using 6-311++G(d,p) basis set can yield adequate and accurate results to calculate ^{14}N and ^{2}H electric field gradients [28,29]. Ida and Wu [36] demonstrated that quantum mechanical calculations at the B3LYP level with both basis sets, 6-31G(f) and 6-311++G(d,p) can yield reliable ^{67}Zn EFG tensors for Zn(II) coordination complexes. To investigate the influence of the metal–ligand interactions on the EFG tensors, all calculations were performed for both of protonation forms and zinc (II) complexes of 4-MeIm.

Following the polarizable continuum model (PCM) developed by Miertus et al. [37], the solvent effects on the EFG tensors was estimated. PCM calculations were performed in the B3LYP level with the 6-311++G(d,p) basis set and using the gas-phase optimized geometries.

4. Results and discussion

First, we attempted to investigate ^{14}N EFG tensors, the nuclear quadrupole coupling constants (χ) and asymmetry parameters (η) for four protonation forms of 4-MeIm as free molecules: the neutral tautomers in which one of the two nitrogen atoms (N1 or N3) is protonated (N1H–MeIm or N3H–MeIm), the fully protonated imidazolium cation (Me-ImH_2^+), and the imidazole anion that is deprotonated at both nitrogen sites (MeIm$^-$). The B3LYP/6-31G(d,p) optimized geometries for these protonation forms are shown in Fig. 1.

Then, we investigated the effect of metal–ligand interactions on the values of χ, η and the EFG tensors of ^{67}Zn, ^{14}N and ^{2}H nuclei, using various Zn(II) complexes of 4-MeIm, where 4-MeIm can be looked upon as a model of histidine. The five complexes considered were the N3–Zn bound and N1 protonated form (N3Zn–N1H–MeIm), the N1–Zn bound and N3 protonated form (N1Zn–N3H–MeIm), the N1–Zn bound imidazolate form (N1Zn–MeIm$^-$), the N3–Zn bound imidazolate form (N3Zn–MeIm$^-$), and the N1, N3–Zn bound imidazolate form (Zn2–MeIm$^-$). Note that the imidazolium cation (N1, N3-protonated) form does not bind to metal ions. Because of its closed shell, the divalent Zn cation was selected as the metal ion, which means that the Zn^{2+}–MeIm complexes have a singlet spin state and hence the computational expense is minimized. Another reason for selecting Zn is that it is found in many mettalloenzyme systems such as carboxy peptidase [9], carbonic anhydrase [10] and superoxide dismutase [11]. The structures of the Zn^{2+}–MeIm complexes depicted in Fig. 2 represent their optimized geometries obtained by the DFT calculations.

4.1. Free molecules

In this part, the DFT calculations at the B3LYP and PW91P86 levels of theory with the 6-311++G(d,p) basis set were carried out to study the protonation and deprotonation effects on the ^{14}N EFG tensors of 4-MeIm. The calculated EFG tensor principal components, q_{ii}, nuclear quadrupole coupling constants, χ, and asymmetry parameters, η, for ^{14}N are summarized in Table 1. With a quick look at the results, some remarkable trends can be observed. Firstly, the EFG tensors for those nuclei change significantly on protonation and deprotanation effects. Secondly, considering the calculated EFG tensors with B3LYP and PW91P86, it is clear that the results obtained with these levels are practically coincident with each other and there is a good agreement with the experimental data [28,17]. The results of B3LYP level are reported in the paper.

As the results in Table 1 indicate, protonation and deprotonation have different influences on the calculated ^{14}N EFG tensors. Protonation causes a decrease in ^{14}N parameters about $\Delta\chi = 1$–2 MHz and $\Delta\eta = 0.08$–0.13. The protonated nitrogen (imino nitrogen) with noticeable $\Delta\chi = 2$ MHz and $\Delta\eta = 0.13$ is the most affected nucleus on protonation. More specifically, for the imino

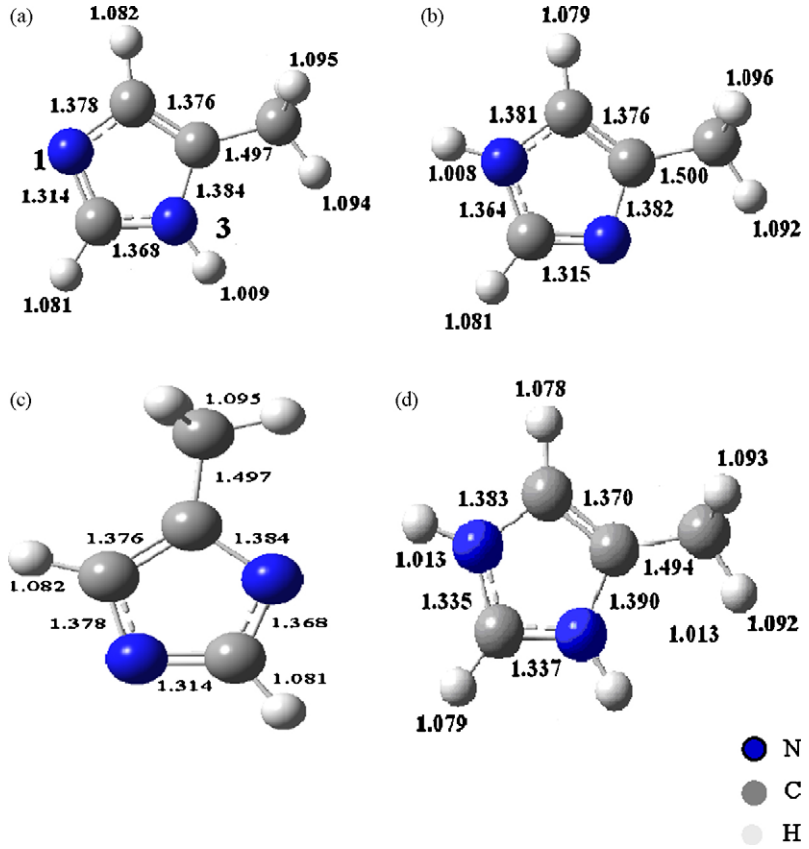

Fig. 1. Optimized geometries and atomic numbering of the four protonation forms of 4-MeIm: (a) N3 protonated form (N3H-MeIm); (b) N1 protonated form (N1H-MeIm); (c) imidazolate anion ($MeIm^-$); and (d) imidazolium cation ($MeImH_2^+$). The atomic numbering indicated in (a) is used for all the four compounds.

Table 1
Calculated[a] EFG tensors of ^{14}N in different protonated forms of 4-MeIm.

Compound	N_{amino}					N_{imino}				
	q_{xx}[b]	q_{yy}[b]	q_{zz}[b]	χ[c]	η	q_{xx}[b]	q_{yy}[b]	q_{zz}[b]	χ[c]	η
N1H–4-MeIm										
Gas	−0.351	−0.262	0.613	2.942	0.150	−0.452	−0.425	0.877	4.210	0.031
	(−0.337)	(−0.249)	(0.586)	(2.812)	(0.150)	(−0.412)	(−0.405)	(0.817)	(3.922)	(0.008)
PCM	−0.289	−0.210	0.450	2.398	0.159	−0.421	−0.399	0.820	3.937	0.026
Exp.				2.524	0.294				4.032	0.120
N3H–4-MeIm										
Gas	−0.369	−0.258	0.627	3.010	0.177	−0.490	−0.416	0.906	4.349	0.082
	(−0.355)	(−0.244)	(0.599)	(2.875)	(0.185)	(−0.442)	(−0.406)	(0.848)	(4.070)	(0.042)
PCM	−0.292	−0.246	0.538	2.582	0.086	−0.444	−0.413	0.857	4.116	0.037
Exp.				2.537	0.178				4.113	0.108
4-MeIm$^-$										
Gas	−0.406	−0.347	0.753	3.614	0.078	−0.402	−0.311	0.713	3.422	0.127
	(−0.393)	(−0.313)	(0.706)	(3.389)	(0.113)	(−0.386)	(−0.276)	(0.662)	(3.178)	(0.166)
PCM	−0.454	−0.366	0.821	3.941	0.107	−0.506	−0.280	0.786	3.773	0.287
4-MeIm$^+$										
Gas	−0.281	−0.189	0.469	2.251	0.169	−0.169	−0.269	0.438	2.102	0.228
	(−0.271)	(−0.187)	(0.458)	(2.198)	(0.183)	(−0.262)	(−0.168)	(0.429)	(2.059)	(0.219)
PCM	−0.293	−0.131	0.424	2.034	0.381	−0.085	−0.289	0.376	1.798	0.543
Histidine										
Gas	−0.335	−0.258	0.593	2.846	0.130	−0.444	−0.430	0.874	4.195	0.016
	(−0.321)	(−0.245)	(0.566)	(2.717)	(0.134)	(−0.418)	−0.396	(0.814)	(3.912)	(0.027)
PCM	−0.285	−0.198	0.483	2.318	0.180	−0.428	−0.373	0.802	3.850	0.069

[a] Results obtained by B3LYP/6-311++G(d,p). Results in parentheses obtained by PW91P86/6-311++G(d,p).
[b] q_{ii} values in atomic units, 1 au = 9.717365×10^{21} V m^{-2}.
[c] Calculated χ values in MHz.

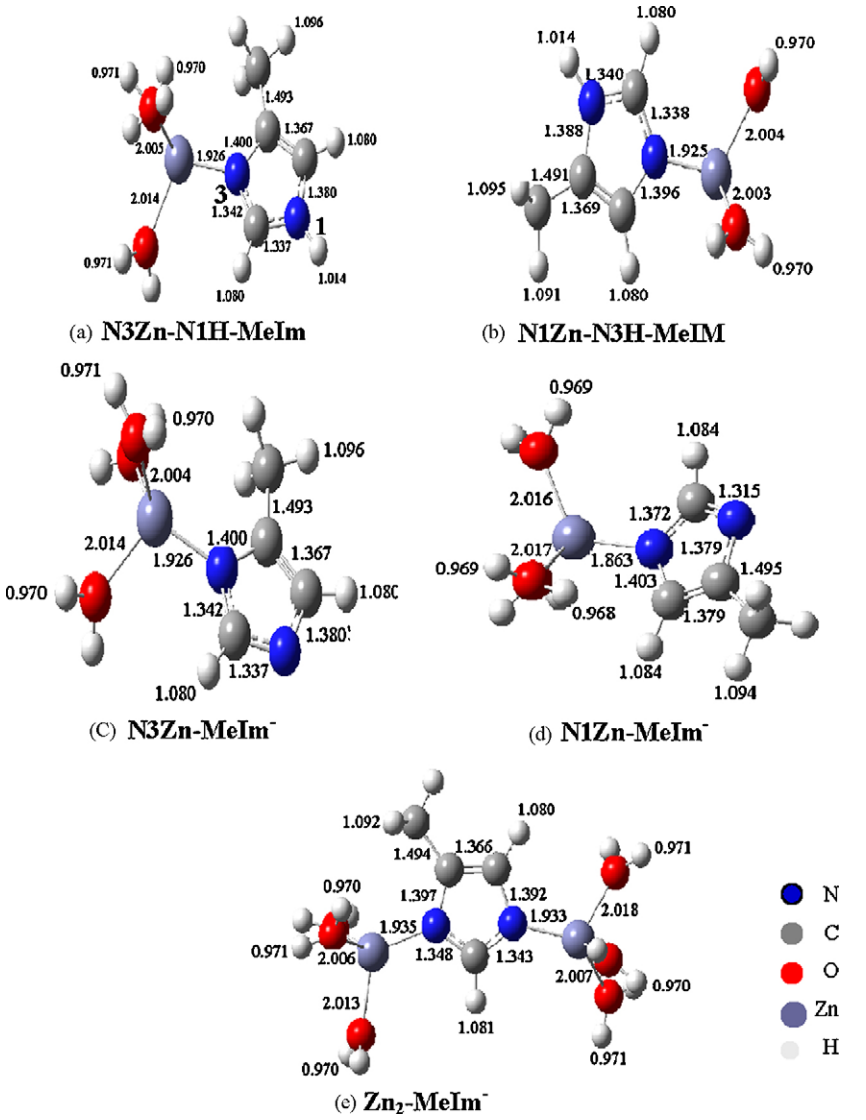

Fig. 2. Optimized geometries of the model Zn (II) complexes of 4-MeIm in different protonation states. The atomic numbering indicated in (a) is used for all the five compounds.

nitrogen, the largest component of the EFG tensor, q_{zz}, changes more noticeably than q_{xx} and q_{yy} through protonation. The values for the q_{zz} tensor element vary by 0.47 but only by 0.15 and 0.30 for the q_{xx} and q_{yy} tensor elements, respectively. The amino nitrogen also shows major changes in the EFG tensors due to the protonation (Table 1). The influence of protonation of the imino nitrogen on the amino nitrogen is revealed by the values of $\Delta\chi$ = 1 MHz and $\Delta\eta$ = 0.08 for the latter. In addition, the results in Table 1 show that deprotonation has a smaller effect on the EFG tensors of nitrogens compared to protonation. It is found that both amino and imino nitrogens with $\Delta\chi$ = 0.5 MHz and $\Delta\eta$ = 0.03–0.1 values change in opposite directions on deprotonation, i. e. unlike amino nitrogens, the EFG tensor elements of imino nitrogens decrease due to deprotonation. The decrease in the EFG tensor elements of imino nitrogens can be a result of delocalized electrons. Two factors control the value of q_{zz} for a quadrupolar nucleus: the charge density at the nucleus and the symmetry of the EFG around the nucleus. Deprotonation of 4-MeIm increases the charge density at both nitrogen atoms. Since the contribution of nonbonding electrons (lone pairs of p and d electrons) to the nonspherical charge distribution is greater than that of bonding electrons, the EFG is more asymmetric in atoms with nonbonding electron pairs due to the increased charge density. On the other hand, if the asymmetry of EFG increases, then q_{zz} and consequently χ would decrease. As a result, the competing effects of charge density and EFG asymmetry on χ offset each other, leading to only a small increase in the χ values of ^{14}N at amino nitrogens and a decrease in the χ values of ^{14}N in the imino nitrogens in the deprotonated form. Thus, we conclude that the ^{14}N χ values are a good marker for distinguishing between the protonation forms. We additionally used the same theoretical method to calculate the EFG tensor of the nitrogen and hydrogen atoms for free histidine (Table 1). The values obtained were very similar to those for free 4-MeIm. This similarity suggests that the general trends reported here for 4-MeIm may be transferred to histidines involved in metal bonding to the nitrogen in a semi-quantitative way.

4.2. Metal–ligand interactions

As mentioned in the previous part, the EFG tensors at the nitrogen site are sensitive to protonation and deprotonation. In this section, the effects of metal–ligand interactions on the ^{14}N, ^{67}Zn

and ^{2}H EFG tensors are discussed. To this aim, B3LYP/6-311++G(d,P) and PW91P86/6-311++G** calculations were carried out for various forms of optimized geometries of Zn(II)–MeIm complexes. The optimized geometries of Zn(II)–MeIm complexes are illustrated in Fig. 2. The calculated EFG tensors, χ and η values for ^{14}N, ^{2}H and ^{67}Zn are summarized in Tables 2–4.

From Table 2, it is seen that the nitrogens are influenced by Zn(II) coordination. Imino nitrogen (proximal nitrogen) with a notable $\Delta\chi$ = 2.9 MHz and $\Delta\eta$ = 0.08 is the most affected atom of 4-MeIm or MeIm anion in the metal–ligand interactions. For this nitrogen atom, all diagonal components of EFG tensors, q_{zz}, q_{xx} and q_{yy} are significant through metal coordination. On the other hand, as a Zn atom is bound to the 4-MeIm, the amino nitrogen (remote nitrogen) shows minor changes in the EFG tensors and $\Delta\chi$ and $\Delta\eta$ values vary by 0.8 MHz and 0.05, respectively. In addition, the results in Table 2 show that the calculated EFG tensors for remote nitrogen display contrasting trends with those values for proximal nitrogen upon Zn binding to $MeIm^{-}$ anion. The EFG tensors of remote nitrogen increase slightly due to metal–ligand interactions. It can be suggested that the unlocalized or nonbonding electron density decreases via metal coordination. The decrease in nonbonding electron density causes an increase in the EFG tensors of remote nitrogen according to the discussion in the previous section. When two Zn atoms are bound to $MeIm^{-}$ at both nitrogen sites, the χ values decrease by $\cong$1.9 MHz at each nitrogen. Moreover, The calculated χ = 1.68 MHz for imino nitrogen and χ = 2.03 MHz for amino nitrogen for Zn(II)–MeIm complexes are expected to be close to experimental values in Zn(II)–Imidazole complexes [38].

Table 3 indicates that the EFG tensors of the amino hydrogen atom in the 4-MeIm change considerably upon Zn binding. $\chi(^{2}H_{amino})$ decreases by 20 KHz, but $\eta(^{2}H_{amino})$ does not alter significantly through metal binding. Furthermore, the present calculations show that upon Zn binding to the neutral forms of 4-MeIm, the N–H distance increases (Fig. 2). The decrease of $\chi(^{2}H_{amino})$ and increase of the N–H distance in 4-MeIm indicate the

Table 2
Calculated[a] EFG tensors of ^{14}N in Zn–MeIm complexes.

Compound	$N_{proximal}$					N_{remote}				
	q_{xx}[b]	q_{yy}[b]	q_{zz}[b]	χ[c]	η	q_{xx}[b]	q_{yy}[b]	q_{zz}[b]	χ[c]	η
N1Zn–n3H–MeIm										
Gas	0.223	0.123	0.346	1.661	0.289	−0.262	−0.191	0.453	2.174	0.156
	(−0.196)	(−0.173)	(0.327)	(1.569)	(0.070)	(−0.251)	(−0.187)	(−0.439)	(−2.107)	(0.145)
PCM	0.310	0.073	−0.383	1.839	0.619	−0.285	−0.166	0.451	2.167	0.264
Exp.				1.604[d]	0.534[d]				2.126[d]	0.567[d]
N3Zn–N1H–MeIm										
Gas	0.196	0.155	−0.351	1.685	0.116	−0.256	−0.168	0.424	2.035	0.207
	(−0.182)	(−0.143)	(0.325)	(1.560)	(0.120)	(−0.248)	(−0.165)	(−0.413)	(1.982)	(0.201)
PCM	0.298	0.088	−0.386	1.853	0.544	−0.269	−0.151	0.420	2.016	0.281
N1Zn–MeIm^{-}										
Gas	−0.342	−0.006	0.348	1.670	0.965	−0.486	−0.404	0.889	4.267	0.092
	(−0.306)	(−0.043)	(0.349)	(1.675)	(0.753)	(−0.431)	(−0.380)	(−0.811)	(3.893)	(0.063)
PCM	0.307	0.089	0.397	1.905	0.548	−0.421	−0.391	0.811	3.895	0.036
N3Zn–MeIm^{-}										
Gas	−0.323	−0.024	0.347	1.665	0.861	0.528	−0.395	0.922	4.425	0.144
	(−0.285)	(−0.065)	(−0.350)	(1.680)	(0.628)	(−0.468)	(−0.380)	(−0.848)	(4.070)	(0.103)
PCM	0.208	0.172	−0.380	1.827	0.093	0.503	−0.427	0.930	4.468	0.081
N1N3Zn$_2$–MeIm^{-}										
Gas	0.206	0.125	−0.332	1.593	0.243	0.183	0.151	−0.334	1.603	0.095
	(−0.159)	(−0.147)	(0.306)	(1.468)	(0.039)	(−0.172)	(−0.134)	(−0.306)	(1.468)	(0.124)
PCM	0.269	0.082	−0.352	1.690	0.531	0.265	0.092	−0.358	1.719	0.481

[a] Results obtained by B3LYP/6-311++G(d,p). Results in parentheses obtained by PW91P86/6-311++G(d,p).
[b] q_{ii} values in atomic units, 1 au = 9.717365 × 10^{21} V m^{-2}.
[c] Calculated χ values in MHz.
[d] Values of χ and η of ^{14}N referred to the experimental data for ^{14}N in imidazolium chloride [38].

Table 3
Calculated[a] EFG tensors of $^{2}H_{amino}$ in Zn–MeIm complexes and the corresponding metal free forms.

Compound	q_{xx}[b]	q_{yy}[b]	q_{zz}[b]	χ[c]	η
N1Zn–N3H–MeIM/N3H–MeIm					
Gas	0.162/0.175	0.216/0.235	−0.379/−0.410	254.69/275.52	0.142/0.146
	(0.166)/(0.179)	(0.217)/(0.235)	(−0.383)/(−0.414)	(257.38)/(278.21)	(0.133)/(0.135)
PCM	0.160/0.170	0.215/0.226	−0.376/−0.396	252.67/266.11	0.146/0.141
N3Zn–N1H–MeIM/N1H–MeIm					
Gas	0.163/0.176	0.216/0.235	−0.379/−0.412	254.69/276.86	0.140/0.143
	(0.166)/(0.180)	(0.216)/(0.235)	(−0.382)/(−0.415)	(256.70)/(278.88)	(0.131)/(0.132)
PCM	0.160/0.170	0.215/0.229	−0.375/−0.399	252.00/268.13	0.147/0.148

[a] Results obtained by B3LYP/6-311++G(d,p). Results in parentheses obtained by PW91P86/6-311++G(d,p).
[b] q_{ii} values in atomic units, 1 au = 9.717365 × 10^{21} V m^{-2}.
[c] Calculated (values in KHz.

Table 4
Calculated[a] EFG tensors of ^{67}Zn in Zn–MeIm complexes.

Compound	q_{xx}[b]	q_{yy}[b]	q_{zz}[b]	(c	(
N1Zn–n3H–MeIm					
Gas	0.544	0.329	0.873	3.076	0.246
	(0.483)	(0.300)	(0.783)	(2.759)	(0.233)
PCM	0.518	0.337	0.85	2.995	0.212
Exp.				2.80[d]	0.4[d]
N3Zn–N1H–MeIm					
Gas	0.585	0.379	0.964	3.397	0.213
	0.530	0.333	0.864	3.045	0.228
PCM	0.498	0.287	0.785	2.766	0.268
N1Zn–MeIm$^-$					
Gas	0.665	0.526	1.191	4.197	0.116
	(0.586)	(0.443)	(1.028)	(3.622)	(0.139)
PCM	0.522	0.601	1.123	3.957	0.070
N3Zn–MeIm$^-$					
Gas	0.701	0.407	1.109	3.908	0.265
	(0.627)	(0.339)	(0.966)	(3.404)	(0.298)
PCM	0.587	0.372	0.959	3.379	0.224
N1N3Zn$_2$–MeIm$^-$					
Gas	0.558/0.604	0.369/0.358	0.927/0.969	3.266/3.390	0.203/0.255
(Zn_1/Zn_2)	(0.495/0.546)	(0.333/0.317)	(0.828/0.863)	(2.917/3.041)	(0.195/0.265)
PCM	(0.508/0.533)	(0.337/0.345)	(0.846/0.879)	(2.981/3.097)	(0.202/0.214)
Zn(H_2O)$_4$					
Gas	0.039	0.036	0.076	0.267	0.028
	(0.042)	(0.039)	(0.082)	(0.288)	(0.036)

[a] Results obtained by B3LYP/6-311++G(d,p). Results in parentheses obtained by PW91P86/6-311++G(d,p).
[b] q_{ii} values in atomic units, 1 au = 9.717365 × 10^{21} V m^{-2}.
[c] Calculated χ values in MHz.
[d] Values of χ and η of ^{67}Zn referred to the experimental data for ^{67}Zn in tetrakis(Imidazole)zincperchlorate [41].

increased acidity of the hydrogen atom in the N–H bond. This metal effect is consistent with the previous calculations by Yazal and Pang [39] in which the proton dissociation energy of imidazole is reduced upon metal binding.

The Zn(II) ion in Zn(H_2O)$_4$ is tetrahedrally coordinated to four water molecules. The EFG in Zn site vanishes due to tetrahedral symmetry or a spherical electron distribution around the Zn(II) ion (Table 4). The four Zn–O bond distances are very similar (1.970 Å). In Zn–MeIm complexes, the Zn–O distances (2.004 Å) are much longer than the Zn–N bonds (1.926 Å). In the imidazole and imidazolate complexes, the distances between the zinc ion and the nitrogen atom in both complexes agree with the average Zn–N distance of 2.1 ± 0.1 Å obtained from the X-ray structures of zinc proteins [40]. The tetrahedral arrangement around the Zn site has been distorted in consequence of coordination to 4-MeIm. As seen from Table 4, the calculated EFG tensors for the Zn site in Zn–MeIm complexes vary significantly due to metal–ligand interactions. The increases of $\chi(^{67}Zn)$ and $\eta(^{67}Zn)$ by 3 MHz and 0.19, respectively reveal the greater influence of metal–ligand interactions on metal. In the Zn–MeIm anion complexes, $\chi(^{67}Zn)$ increases by 4 MHz more than in the Zn–MeIm complexes, which indicates the deprotonation effect on metal–ligand interactions. This implies a potential role of the 4-MeIm or histidine ligand in managing the catalytic reactions of metalloenzymes by changing its protonation state. As two Zn atoms are bound to $MeIm^-$ at both nitrogen sites, the calculated EFG tensors show deviations from axial symmetry in both Zn sites. The $\chi(^{67}Zn)$ values increase around 3 MHz at each Zn site. The calculated $\chi(^{67}Zn)$ shows a good agreement with experimental data reported for Zn–imidazole complexes [36,41].

4.3. Simulation of the solvent effect

Water is an important component in biological systems, and it affects protein–protein and protein–nucleic acid interactions in metalloenzyme reactions. In the present work, the long-range effects of water on the EFG tensors of the studied nuclei have been considered. PCM was used to reproduce the electronic environment in solution by a continuum of ε = 78.3. The computed values are gathered in Tables 1–4. Comparison of the gas phase and PCM for different forms of 4-MeIm shows that the long-range effects change the EFG around nitrogen atoms in 4-MeIm. This change is more important for amino nitrogens. These results are in agreement with previous studies for imidazole derivatives [28]. Furthermore, it is interesting to consider solvent effects on the electronic environment of Zn–MeIm complexes. For this purpose, we performed PCM calculations for different forms of Zn–MeIm complexes. The results in Table 2 show that inclusion of PCM has a reverse effect on the χ values of nitrogens. The χ values of proximal nitrogens increase as a result of solvent effects, while the χ values of remote nitrogens decrease due to these effects. In addition, the results indicate that the changes of χ values of zinc from the gas phase to solution are about 10% (Table 4). The values of χ are reduced in solution, as expected.

Table 5
Calculated[a] EFG tensors of ^{67}Zn and ^{14}N for model superoxide dismutase in the gas phase.

Nucleus	q_{xx}[b]	q_{yy}[b]	q_{zz}[b]	χ[c]	η
Zn	0.141	0.222	−0.363	1.278	0.223
	(0.125)	(0.203)	(−0.328)	(1.154)	(0.238)
$N_{proximal}$	−0.032	−0.374	0.406	1.949	0.842
	(−0.004)	(−0.352)	(0.356)	(1.709)	(0.977)
N_{remote}	−0.265	−0.23	0.496	2.381	0.070
	(−0.225)	(−0.254)	(0.480)	(2.304)	(0.060)

[a] Results obtained by B3LYP/6-311++G(d,p). Results in parentheses obtained by PW91P86/6-311++G(d,p).
[b] q_{ii} values in atomic units, 1 au = 9.717365 × 10^{21} V m^{-2}.
[c] Calculated χ values in MHz.

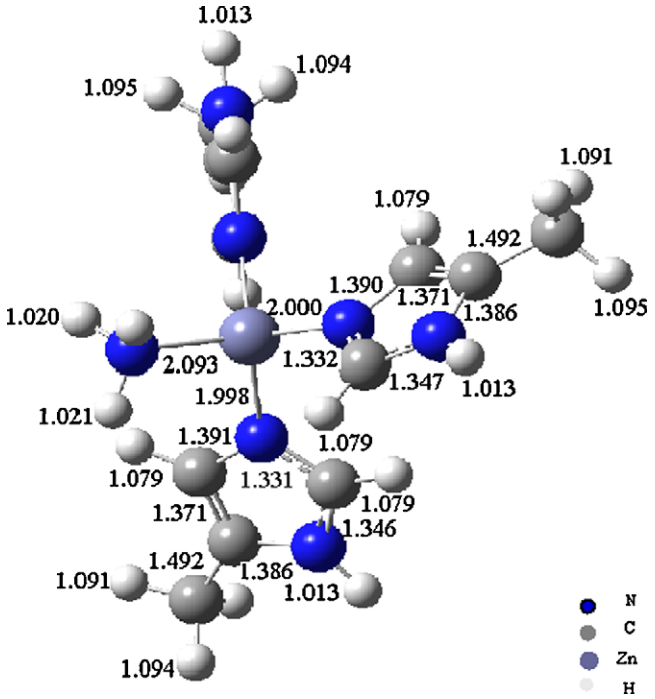

Fig. 3. Optimized geometry for simplified model of superoxide dismutase.

4.4. Simulation of the metal–ligand interactions in superoxide dismutase

The crystallographic structures of superoxide dismutase show that the Zn(II) ion is coordinated by three histidine residues and an aspartate in a distorted tetrahedron [11]. Up to this point, a simple model for superoxide dismutase has been employed, using 4-MeIm and NH_3 instead of histidine and aspartate residues, respectively (Fig. 3). Table 5 displays the EFG tensor components, χ and η for ^{14}N and ^{67}Zn corresponding to the model of superoxide dismutase. In this model, the results of χ and η values for proximal and remote nitrogens are consistent with a much larger distortion of electron distribution around proximal nitrogens than remote nitrogens due to the presence of the metal ion. These results are in agreement with those in coenzyme B12 reported by Morokuma et al. [28]. The $\chi(^{67}Zn) = 1.28$ MHz and $\eta(^{67}Zn) = 0.22$ confirm the distortion around Zn from tetrahedral symmetry.

5. Conclusion

Based on DFT calculations, it is concluded that the EFG tensors of nitrogen atoms are good indicators to characterize the different protonation forms of 4-MeIm and the properties of metal–ligand interactions. The EFG tensors of imino and amino nitrogens change significantly through protonation, but deprotonation has a minor effect on them. The results show that the electronic environments of both metal and ligand are affected by metal–ligand interactions. The binding of Zn(II) to 4-MeIm or $MeIm^-$ anion causes notable changes in the EFG tensors of proximal nitrogens with respect to remote nitrogens. The increase in the χ of Zn site is ≅3.39 MHz for Zn–MeIm complexes, while this value becomes ≅4.19 MHz for Zn–$MeIm^-$ anion complexes. This means that protonation state of 4-MeIm or histidine ligand can alter the electronic environment of the binding metal ion. This effect is important in controlling the catalytic reactions in some metalloenzymes. Insertion of solvent effects leads to significant changes in the electronic environment of nitrogen, amino hydrogen and zinc atoms. In this work, we estimated NQR parameters of proximal nitrogens ($\chi(^{14}N) = 1.95$ MHz and $\eta(^{14}N) = 0.84$), remote nitrogens($\chi(^{14}N) = 2.38$ MHz and $\eta(^{14}N) = 0.07$), and zinc ion ($\chi(^{67}Zn) = 1.28$ MHz and $\eta(^{67}Zn) = 0.22$) in superoxide dismutase.

References

[1] E.I. Ochiai, D.H. Busch, H. Shull, in: Allyn, Bacon (Eds.), Bioinorganic Chemistry: An Introduction, Boston, 1977.
[2] S. Scheiner, M. Yi, Proton transfer properties of imidazole, J. Phys. Chem. 100 (1996) 9235–9241.
[3] C.A. Lesburg, D.W. Christianson, X-ray crystallographic studies of engineered hydrogen bond networks in a protein–zinc binding site, J. Am. Chem. Soc. 117 (1995) 6838–6844.
[4] S.B. Vik, B.J. Antonio, A mechanism of proton translocation by F1F0 ATP synthases suggested by double mutants of the a subunit, J. Biol. Chem. 269 (1994) 30364–30369.
[5] R. Hienerwadel, C. Berthomieu, Bicarbonate binding to the non-heme iron of photosystem II investigated by Fourier transform infrared difference spectroscopy and ^{13}C-labeled bicarbonate, Biochemistry 34 (1995) 16288–16297.
[6] C. Berthomieu, R. Hienerwadel, Iron coordination in photosystem. II: interaction between bicarbonate and the Q_B pocket studied by Fourier transform infrared spectroscopy, Biochemistry 40 (2001) 4044–4052.
[7] L.M. Hansen, A. Derecskei-Kovacs, D.S. Marynick, Electronic structure of the coenzyme vitamin B_{12} and related systems. Part II: A Corrin model system, J. Mol. Struct. 431 (1998) 53–57.
[8] C. Mealli, M. Sabat, L.G.A. Marzilli, Coenzyme B_{12} Co–C bond homolysis: Insights from qualitative molecular orbital theory, J. Am. Chem. Soc. 109 (1987) 1593–1594.
[9] D.M. Hayes, P.A. Kollman, Electrostatic potentials of proteins. 1. Carboxypeptidase A, J. Am. Chem. Soc. 98 (1976) 3335–3343.
[10] J.M. Harrowfield, V. Norris, A.M. Sargeson, Reactivity of coordinated nucleophiles. A comparison of metal bound imidazolate and hydroxide ions as models for carbonic anhydrase, J. Am. Chem. Soc. 98 (1976) 7282–7289.
[11] L.M. Murphy, R.W. Strange, S.S. Hasnain, A critical assessment of the evidence from XAFS and crystallography for the breakage of the imidazolate bridge during catalysis in CuZn superoxide dismutase, Structure 5 (1997) 371–379.
[12] Y. Wei, A.C.D. Dios, A.E.M. Dermott, Solid-state ^{15}N NMR chemical shift anisotropy of histidines: experimental and theoretical studies of hydrogen bonding, J. Am. Chem. Soc. 121 (1999) 10389–10394.
[13] C.I.H. Ashby, C.P. Cheng, T.L. Brown, Nitrogen-14 nuclear quadrupole resonance spectra of coordinated imidazole, J. Am. Chem. Soc. 100 (1978) 6057–6063.
[14] K. Hasegawa, T.-A. Ono, T. Noguchi, Vibrational spectra and ab initio DFT calculations of 4-methylimidazole and its different protonation forms: infrared and Raman markers of the protonation state of a histidine side chain, J. Phys. Chem. B 104 (2000) 4253–4265.
[15] A. Toyama, K. Ono, S. Hashimoto, H. Takeuchi, Raman spectra and normal coordinate analysis of the N1-H and N3-H tautomers of 4-methylimidazole: vibrational modes of histidine tautomer markers, J. Phys. Chem. A 106 (2002) 3403–3412.
[16] S. Hashimoto, H. Takeuchi, Detection of UV resonance Raman bands of the distal histidine in cyanide-bound horseradish peroxidase: evidence for two hydrogen-bonding states of the imidazolium side chain, J. Am. Chem. Soc. 120 (1998) 11012–11013.
[17] T. Ueda, Sh. Nagatomo, H. Masui, N. Nakamura, Hydrogen bonds in crystalline imidazoles studied by ^{15}N NMR and ab initio MO calculations, Z. Naturforsch. 54a (1999) 437–442.
[18] H. Gallouj, P. Lagant, G. Vorgoten, A force field derived by density functional theory for 4-ethylimidazole: use of the ultraviolet resonance Raman intensities to check the vibrational analysis, J. Raman Spectrosc. 28 (1997) 909–916.
[19] M. Majoube, Ph. Millié, G. Vergoten, Vibrational spectra of 4-methylimidazole: assignment of modes and calculation of Raman and resonance Raman intensities at the ab initio 6-31G level, J. Mol. Struct. 344 (1995) 21–36.
[20] K. Hasegawa, T.-A. Ono, T. Noguchi, Ab initio density functional theory calculations and vibrational analysis of zinc-bound 4-methylimidazole as a model of a histidine ligand in metalloenzymes, J. Phys. Chem. A106 (2002) 3377–3390.
[21] C.I.H. Ashby, W.F. Paton, T.L. Brown, Nitrogen-14 nuclear quadrupole resonance spectra of the coordinated amino group and of coordinated imidazole: Crystal and molecular structures of chloroglycylglycinato(imidazole)cadmium, J. Am. Chem. Soc. 102 (1980) 2990–2998.
[22] J.D. Graybeal, Molecular Spectroscopy, McGraw-Hill, New York, 1998.
[23] T.P. Das, E.L. Han, Nuclear Quadrupole Resonance Spectroscopy, Academic Press, New York, 1958.
[24] J. Fritscher, Influence of hydrogen bond geometry on quadrupole coupling parameters: a theoretical study of imidazole-water and imidazole-semiquinone complexes, Phys. Chem. Chem. Phys. 6 (2004) 4950–4956.
[25] S.K. Amini, N.L. Hadipour, F. Elmi, Study of hydrogen bond of imidazole and its 4-nitro derivative by ab initio and DFT calculated NQR parameters, Chem. Phys. Lett. 391 (2004) 95–100.
[26] N. Nakamura, H. Masui, T. Ueda, Effect of intermolecular hydrogen bonding on the nuclear quadrupole interaction in imidazole and its derivatives as studied by *ab initio* molecular orbital calculations, Z. Natureforsch. 55a (2000) 315–322.

[27] J.N. Latosińska, J. Seliger, B. Nogaj, Electron density distribution in 2-nitro-5-methylimidazole derivatives studied by NMR-NQR double resonance, Magn. Rosen. Chem. 37 (1999) 878–880.
[28] M. Torrent, D.G. Musaev, K. Morokuma, Calculation of nuclear quadrupole parameters in Imidazole derivatives and extrapolation to coenzyme B_{12}. A theoretical study, J. Phys. Chem. B 103 (1999) 8618–8627.
[29] S.M. Nasseri, N.L. Hadipour, A.R. Mohebbi, A density functional study of ^{14}N NQR parameters of imidazole derivatives and extrapolation to PfHRP2–Fe^{3+}-PPIX complex, J. Mol. Struct. 820 (2007) 48–52.
[30] E.A.C. Lucken, Nuclear Quadrupole Coupling Constants, Academic Press, London, 1992.
[31] P. Pyykkö, Spectroscopic nuclear quadrupole moment, Mol. Phys. 99 (2001) 1617–1629.
[32] M.J. Frisch, G.W. Trucks, H.B. Schlegel, G.E. Scuseria, M.A. Robb, J.R. Cheeseman, V.G. Zakrzewski, J.A. Montgomery Jr., R.E. Stramann, J.C. Burant, S. Dapprich, J.M. Millam, A.D. Daniels, K.N. Kudin, M.C. Strain, O. Farkas, J. Tomasi, V. Barone, M. Cossi, R. Commi, B. Mennucci, C. Pomelli, C. Adamo, S. Cliffod, J. Ochterski, G.A. Peterson, P.Y. Ayaly, Q. Cui, K. Morokuma, D.K. Malick, A.D. Rabuck, K. Raghavachari, J.B. Foresman, J. Ciolowski, J.V. Oriz, B.B. Stefanov, G. Liu, A. Liashenko, P. Piskorz, I. Komaromi, R. Gomperts, R.L. Martin, D.J. Fox, T. Keith, M.A. Al-Laham, C.Y. Peng, A. Nanayakkara, C. Gonzalez, M. Challacomb, P.M.W. Gill, B. Johnson, W. Chen, M.W. Wong, J.L. Andres, C. Gonzales, M. Head-Gordon, E.S. Replogle, J.A. Pople, Gausssian 98, Gaussian, Inc., Pittsburg, PA, 1998.
[33] A.D. Becke, Density-functional thermochemistry. 3. The role of exact exchange, J. Chem. Phys. 98 (1993) 5648–5652.
[34] C. Lee, W. Yang, R.G. Parr, Development of the colle-salvetti correlation—energy formula in to a functional of the electron density, Phys. Rev. B 37 (1988) 785–789.
[35] J.P. Perdew, J.A. Chevary, S.H. Vosko, K.A. Jackson, M.R. Pederson, D.J. Singh, C. Fiolhais, Atoms, molecules, solids, and surfaces: applications of the generalized gradient approximation for exchange and correlation, Phys. Rev. B 46 (1992) 6671–6687.
[36] R. Ida, G. Wu, Theoretical study of the ^{67}Zn electric-field gradient tensors in zinc(II) coordination complexes, J. Phys. Chem. A 106 (2002) 11234–11239.
[37] S. Miertus, E. Scrocco, J. Tomasi, Electrostatic interaction of a solute with a continuum. A direct utilizaion of AB initio molecular potentials for the prevision of solvent effects, Chem. Phys. 55 (1981) 117–129.
[38] G.I.H. Ashby, C.P. Cheng, T.L. Brown, ^{14}N nuclear quadrupole resonance spectra of coordinated imidazole, J. Am. Chem. Soc. 100 (1978) 6057–6063.
[39] J.E. Yazal, Y.-P. Pang, Ab initio calculations of proton dissociation energies of zinc ligands: hypothesis of imidazole as zinc ligand in proteins, J. Phys. Chem. B 103 (1999) 8773–8779.
[40] R.R. Roe, Y.-P. Pang, Zinc's exclusive tetrahedral coordination governed by its electronic structure, J. Mol. Model. 5 (1999) 134–140.
[41] Y. Zhang, S. Mukherjee, E. Oldfield, ^{67}Zn NMR chemical shifts and electric field gradients in zinc complexes: a quantum chemical investigation, J. Am. Chem. Soc. 127 (2005) 2370–2371.